AIP Journal of Renewable and Sustainable Energy

A first-principles density functional theory study of the electronic structural and thermodynamic properties of M2ZrO3 and M2CO3 (M=Na, K) and their capabilities for CO2 capture

Yuhua Duan

Citation: J. Renewable Sustainable Energy **4**, 013109 (2012); doi: 10.1063/1.3683519
View online: http://dx.doi.org/10.1063/1.3683519
View Table of Contents: http://jrse.aip.org/resource/1/JRSEBH/v4/i1
Published by the American Institute of Physics.

A first-principles density functional theory study of the electronic structural and thermodynamic properties of M_2ZrO_3 and M_2CO_3 (M = Na, K) and their capabilities for CO_2 capture

Yuhua Duan[a)]
National Energy Technology Laboratory, United States Department of Energy, Pittsburgh, Pennsylvania 15236, USA

(Received 28 June 2011; accepted 2 January 2012; published online 8 February 2012)

Alkali metal zirconates could be used as solid sorbents for CO_2 capture. The structural, electronic, and phonon properties of Na_2ZrO_3, K_2ZrO_3, Na_2CO_3, and K_2CO_3 are investigated by combining the density functional theory with lattice phonon dynamics. The thermodynamics of CO_2 absorption/desorption reactions of these two zirconates are analyzed. The calculated results show that their optimized structures are in a good agreement with experimental measurements. The calculated band gaps are 4.339 eV (indirect), 3.641 eV (direct), 3.935 eV (indirect), and 3.697 eV (direct) for Na_2ZrO_3, K_2ZrO_3, Na_2CO_3, and K_2CO_3, respectively. The calculated phonon dispersions and phonon density of states for M_2ZrO_3 and M_2CO_3 (M = K, Na, Li) revealed that from K to Na to Li, their frequency peaks are shifted to high frequencies due to the molecular weight decreased from K to Li. From the calculated reaction heats and relationships of free energy change versus temperatures and CO_2 pressures of the M_2ZrO_3 (M = K, Na, Li) reacting with CO_2, we found that the performance of Na_2ZrO_3 capturing CO_2 is similar to that of Li_2ZrO_3 and is better than that of K_2ZrO_3. Therefore, Na_2ZrO_3 and Li_2ZrO_3 are good candidates of high temperature CO_2 sorbents and could be used for post-combustion CO_2 capture technologies. [doi:10.1063/1.3683519]

I. INTRODUCTION

Nowadays, the burning of fossil fuels is the main energy source for the world economy. One consequence of the use of these carbon based fuels is the emission of huge quantities of CO_2 into the atmosphere creating environmental problems such as global climate warming.[1–4] In order to solve such environmental problem and to stop emission, the CO_2 must be captured and sequestered underground.[5,6] During past few decades, many efforts have been devoted to develop new technologies for CO_2 capture, sequestration, and utilization for improving energy efficiency.[7] Among them, capture is the key technology in which the effective sorbent materials must be available. Current CO_2 capture technologies for power generation processes including amine solvents and CaO-based sorbent materials require very energy intensive regeneration steps which result in significantly decreased efficiency. Hence, there is a critical need for new materials that can capture and release CO_2 reversibly with acceptable energy costs if CO_2 is to be captured and sequestered economically.

Inorganic sorbents are one such class of materials which typically capture CO_2 through the reversible formation of carbonates. Recent experimental investigations found that alkali metal silicates and zirconates are good candidates of solid sorbents for CO_2 capture in terms of large CO_2 sorption capacity, infinite CO_2/N_2 or CO_2/H_2 selectivity, good reversibility, and high

[a)]Author to whom correspondence should be addressed. Electronic mail: yuhua.duan@netl.doe.gov. Tel.: 412-386-5771. Fax: 412-386-5920.

operating temperature.[8–13] As described in our previous paper,[14] in the literature, there are many experimental works on Li_2ZrO_3 capture CO_2, but only have few reports on CO_2 capture by Na_2ZrO_3 and K_2ZrO_3. Lopez-Ortiz *et al.*[15] compared the CO_2 capture performance of Na_2ZrO_3 with Li_2ZrO_3 and Li_4SiO_4 and found that Na_2ZrO_3 has better performance. Their experimental data showed that Na_2ZrO_3 presented highest sorption rate and can absorb almost 100% of the maximum theoretical CO_2 sorption compared to 70% and 80% of Li_2ZrO_3 and Li_4SiO_4. Their results also indicated the regeneration performance of Na_2ZrO_3 was not as good as Li_4SiO_4 and Li_2ZrO_3. Zhao *et al.*[16] investigated the kinetics of the CO_2 capture properties of nanocrystalline Na_2ZrO_3 and found that monoclinic Na_2ZrO_3 is much more active than its hexagonal counterpart. Their results showed that nanocrystalline Na_2ZrO_3 is a very promising CO_2 acceptor for different applications due to its excellent stability and durability[17] and to be able to work at CO_2 partial pressure as low as 0.025 bar. Based on measuring the isotherms of CO_2 sorption and kinetic analysis, Alcerreca-Corte *et al.*[18] investigated the CO_2 absorption on Na_2ZrO_3 and found that there are two different processes taking place: (1) CO_2 chemsorption over surface of the particles; (2) once the Na_2CO_3 shell formed, the second process of Na diffusion from core of the particles to the surface to reactive the first chemsorption process. Obviously, the second step is the limiting step of the total absorption process as the estimated activation energies of these two steps are 33.866 kJ/mol and 48.009 kJ/mol, respectively. Sandoval-Diaz and Pfeiffer[19] explored the effects of CO_2 chemsorption of K-doped Na_2ZrO_3 and found that doped-K enhanced the CO_2 chemsorption and diffusion kinetics of Na_2ZrO_3 and the 40% doping rate give the best solid solution for the CO_2 capture. Ochoa-Fernandez *et al.*[20] explored the effects of steam addition on the properties of high temperature ceramic CO_2 acceptors and found that the presence of water in the form of steam enhances the capture and regeneration rates but has a large decay in capacity compared to the performance at dry conditions. Velderrain *et al.*[21] found that small portion of Li addition could increase the absorption capacity of Na_2ZrO_3, but too much Li (>25% mol) will decrease its absorption capacity. Although the K_2ZrO_3 is a stable solid material and there are several reports on K-doped Li_2ZrO_3 and Na_2ZrO_3 sorbents,[10,19,20,22–24] no report on the performance of pure K_2ZrO_3 capture CO_2 was found in the literature. Therefore, it is worthwhile to investigate the CO_2 capture behaviors of K_2ZrO_3 and provide the comparison with Li_2ZrO_3 and Na_2ZrO_3.

Computational modeling could play an important role in developing new CO_2 sorbents by identifying the corresponding thermodynamic and kinetic characteristics of the sorbent materials of interest.[25] In order to identify optimum candidates for CO_2 solid sorbents (that can be further subjected to experimental testing) from vast of solid materials, we have developed a multi-step computational methodology based on combining the first principles' calculations with lattice phonon dynamics to describe the thermodynamic properties of CO_2 capture reactions by solid sorbents.[26–28] In the literature, there are few theoretical studies, particularly on the electronic structure and lattice dynamics of the alkali metal zirconates. In our previous study,[14] we explored the CO_2 capturing properties of Li_2ZrO_3 and $Li_6Zr_2O_7$ and found that the performance of Li_2ZrO_3 as a CO_2 sorbent is better than that of $Li_6Zr_2O_7$. In the first half cycle, sorbents absorbing CO_2 to form lithium carbonate, $Li_6Zr_2O_7$ performs better than Li_2ZrO_3 because the former releases more heat of reaction and has a lower Gibbs free energy and a higher CO_2 capture capacity. However, during the second half cycle, regenerating sorbent from carbonate and zirconia to release CO_2, the main product is the thermodynamically favorable Li_2ZrO_3 rather than forming $Li_6Zr_2O_7$. These results are in a good agreement with experimental findings.[5] Following our previous study of lithium zirconates capture CO_2,[14] in this study, we use same procedure to investigate the electronic structural and the lattice dynamical phonon properties of M_2ZrO_3 and M_2CO_3 (M = Na, K) extensively. Then, compared with Li_2ZrO_3, we analyze in detail their properties of CO_2 absorption/desorption based on the calculated energetic and thermodynamic results from the obtained electronic structural and phonon dynamical properties.

The remainder of this report is organized as follows: In Sec. II, we briefly describe the theoretical method we employed. In Sec. III, we present the electronic and phonon results for these alkali metal zirconates and carbonates and compare them with other available data. Subsequently, compared with Li_2ZrO_3, we analyze their capabilities for CO_2 capture by calculating

the chemical potential change for the capture reactions under different external pressures and temperatures. And in Sec. IV, we summarize our conclusions.

II. THEORETICAL METHODS

The complete description of our computational methodology can be found in our previous papers.[14,26–29] Here, we limit ourselves to provide only the main aspects relevant for the current study. When applying the alkali metal zirconates as solid CO_2 absorbents, we have the following reactions:

$$M_2ZrO_3 + CO_2 \overset{T,P}{\longleftrightarrow} M_2CO_3 + ZrO_2 \quad (M = K, Na, Li). \tag{1}$$

Assuming the difference between the chemical potential of solid phases (M_2ZrO_3, ZrO_2, and M_2CO_3) can be approximated by the differences in their electronic energies (ΔE^{DFT}) and their entropies (ΔS_{PH}) and harmonic free energies (ΔF_{PH}), we can obtain the temperature and pressure dependent chemical potential ($\Delta\mu$) for these reactions[14,28–31]

$$\Delta\mu(T,P) = \Delta\mu^0(T) - RT\ln\left(\frac{P_{CO_2}}{P_0}\right), \tag{2}$$

with

$$\Delta\mu^0(T) = \Delta E^{DFT} + \Delta E_{ZP} + \Delta F_{PH}(T) - G_{CO_2}(T), \tag{3}$$

where ΔE_{ZP} is the zero point energy difference between the reactants and products and can be obtained directly from phonon calculations. P_0 is the standard state reference pressure of 1 bar. (Note that in our previous paper,[14] in Eq. (3) there is a typo error with an extra term $-T\Delta S_{PH}(T)$.) The enthalpy change for the reactions (1), $\Delta H^{cal}(T)$, can be derived from above equations as

$$\Delta H^{cal}(T) = \Delta\mu^0(T) + T(\Delta S_{PH}(T) - S_{CO_2}(T)). \tag{4}$$

As described in our previous study,[14,27,28] the zero-point energy, the free energy and the entropy of CO_2 ($E_{zp\_CO_2}$, $G_{CO_2}(T)$, $S_{CO_2}(T)$) can be obtained by standard statistical mechanics and accurately evaluated using the Shomate equation. In Eq. (3), ΔE^{DFT} is the total energy change of the reactants and products calculated by density functional theory (DFT). In this work, the Vienna *Ab-initio* Simulation Package (VASP)[32,33] was employed to calculate the electronic structures of the solid materials involved in this study. All calculations have been done using the projector augmented wave (PAW), pseudo-potentials, and the PW91 exchange-correlation functional.[34] This computational level was shown to provide an accurate description of oxide systems.[28,29,35] Plane wave basis sets were used with a cutoff energy of 500 eV and a kinetic energy cutoff for augmentation charges of 605.4 eV. The k-point sampling grids of $n_1 \times n_2 \times n_3$, obtained using the Monkhorst-Pack method,[36] were used for these bulk calculations, where n_1, n_2, and n_3 were determined consistent to a spacing of about 0.028 $Å^{-1}$ along the axes of the reciprocal unit cells. The corresponding k-points sets that we used in our calculations were $7 \times 4 \times 4$ for Na_2ZrO_3, $6 \times 3 \times 5$ for K_2ZrO_3, $4 \times 8 \times 6$ for Na_2CO_3, and $6 \times 4 \times 6$ for K_2CO_3, respectively. The valence electrons contain the *s* and *p* orbitals of Na, C, and O atoms, and the *s*, *p*, and *d* orbitals of K and Zr. During the calculations, all atoms in the cell as well as the lattice dimensions and angles were relaxed to the equilibrium configurations. For band structure and phonon dispersion calculations, the symbols and coordinates of the high symmetrical points in the first Brillouin zone of the crystals are taken from Bradley and Cracknell's definitions.[37]

In Eqs. (3) and (4), the zero-point-energies (E_{ZP}), entropies (S_{PH}), and harmonic free energies (F_{PH}, excluding zero-point energy which was already counted into the term ΔE_{Zp}) of solids were calculated by the PHONON software package[38] in which the direct method is applied following the formula derived by Parlinski *et al.*[39] to combine *ab initio* DFT with lattice phonon

dynamics calculations. In the phonon calculations, a $2 \times 1 \times 1$ supercell is created for Na_2ZrO_3 and a $2 \times 1 \times 2$ supercell for K_2ZrO_3 from their optimized unit cells that are calculated through DFT while a $2 \times 2 \times 2$ supercell for M_2CO_3 (M = Na, K) is created for phonon calculations. Based on the partition function carried out with the phonon dispersions and phonon densities of states, their thermodynamic properties, such as internal energy, free energy, entropy, heat capacity, etc., can be evaluated under different temperature and pressure that are used in Eq. (2) to calculate the chemical potentials for the reaction (1).

III. RESULTS AND DISCUSSIONS

A. Structural optimization and electronic structural properties

Experimentally, with different M_2CO_3/ZrO_2 ratios (where M = Li, Na, K), the alkali metal zirconates are synthesized by reacting alkali carbonates M_2CO_3 with ZrO_2 at high temperature.[40–42] Figure 1 shows the crystal structures of these four crystals which are studied in this work. As Bastow *et al.*[40] measured and shown in Fig. 1(a), the structure of Na_2ZrO_3 is isotypic with Li_2SnO_3 (Ref. 43) and Li_2TiO_3,[44] crystallizing in a monoclinic space group C2/c (#15) with unit cell parameters a = 5.623 Å, b = 9.749 Å, c = 11.127 Å, and $\beta = 99.98°$, and with eight formula units (f.u.) per unit cell. However, K_2ZrO_3 is in the orthorhombic system *Pnma* (#62) with unit cell dimensions of $a = 5.93$ Å, $b = 10.48$ Å, and $c = 7.03$ Å (shown in Fig. 1(b)).[41,42] Its structure contains chains of edge-sharing ZrO_5 square pyramids, with apices oppositely directed, running in the x direction. Their experimental crystal structural constants as well as our optimized structural constants of Na_2ZrO_3 and K_2ZrO_3 are summarized in Table I. Although the experimental measurements showed that the Na_2CO_3 and K_2CO_3 could have

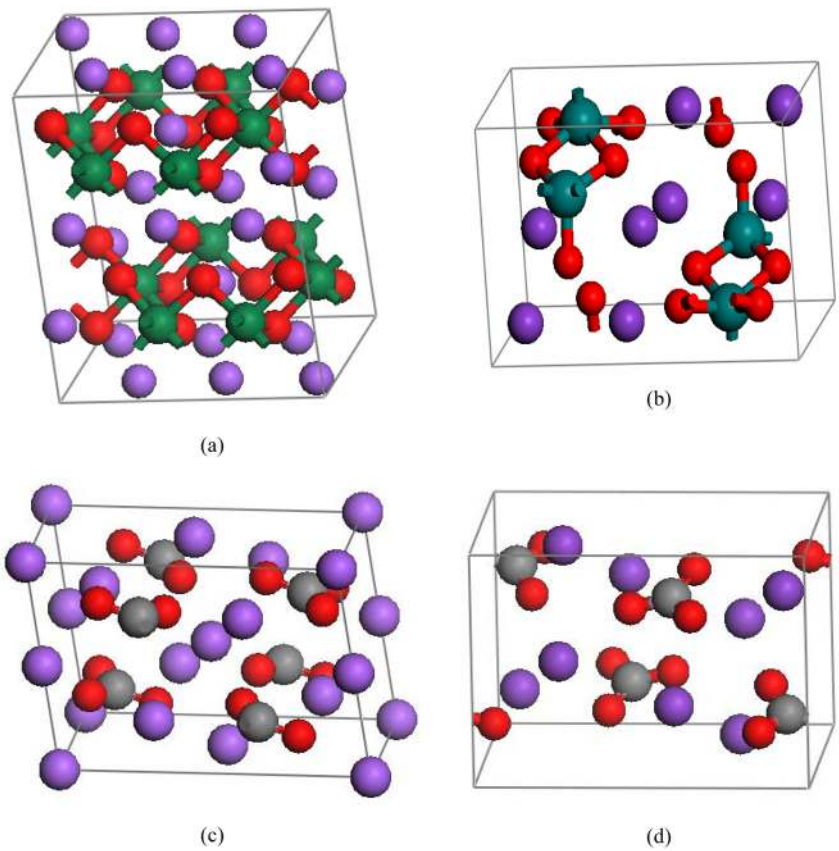

FIG. 1. The crystal structures of sodium and potassium zirconates and carbonates. Biggest ball stands for Zr in green or C in gray, smallest in red for O, purple for Na or K. c axis is vertical. (a) Na_2ZrO_3 in space group C12/c1(No.15); (b) K_2ZrO_3 in space group Pnma(No.62); (c) Na_2CO_3 in space group C12/m1(No.14); (d) K_2CO_3 in space group $P12_1/c1$(No.14).

TABLE I. The experimental and optimized crystal structural constants of M_2ZrO_3 and M_2CO_3 (M = Na, K), with all distances in angstroms (Å) and angles in degrees.

	Lattice constants			Fractional coordinates	
Crystal and space group	Experimental	Optimized	Deviation (%)	Experimental	Optimized
Na_2ZrO_3 C12/c1(No.15)[a] f.u. = 8	a = 5.623	5.612809	−0.18	Na: (0.238, 0.077,−0.0001)	Na: (0.236467, 0.078715, −0.000236)
	b = 9.749	9.735747	−0.14	(0.250, 0.250, 0.500)	(0.250000, 0.250000, 0.500000)
	c = 11.127	10.95675	−1.53	(0.000, 0.085, 0.250)	(0.000000, 0.084843, 0.250000)
	β = 99.98°	100.0426°	0.01	Zr: (0.000, 0.415, 0.250)	Zr: (0.000000, 0.417918, 0.250000)
				(0.000, 0.747, 0.250)	(0.000000, 0.750255, 0.250000)
				O: (0.141, 0.265, 0.138)	O: (0.147306, 0.268494, 0.142479)
				(0.102, 0.586, 0.138)	(0.096802, 0.584613, 0.142216)
				(0.138, 0.906, 0.135)	(0.145907, 0.901650, 0.140869)
K_2ZrO_3 Pnma(No.62)[b] f.u. = 4	a = 5.93	5.945627	0.26	K: (0.264, 0.5857, 0.1143)	K: (0.264974, 0.585884, 0.113494)
	b = 10.48	10.63924	1.52	Zr: (0.2730, 0.25, 0.1598)	Zr: (0.278576, 0.250000, 0.159942)
	c = 7.03	7.116156	1.23	O: (0.175, 0.75, 0.390)	O: (0.159605, 0.750000, 0.391444)
				(0.015, 0.121, 0.234)	(0.016177, 0.122053, 0.229819)
Na_2CO_3 C12/m1(No.12)[c] f.u. = 4	a = 8.99881	8.95180	−0.52	Na: (0.0000, 0.0000, 0.0000)	Na: (0.000000, 0.000000, 0.000000)
	b = 5.24381	5.33507	1.74	(0.0000, 0.0000, 0.5000)	(0.000000, 0.000000, 0.500000)
	c = 6.2868	6.13861	−2.36	(0.168, 0.5000, 0.7511)	(0.170359, 0.500000, 0.746427)
	β = 97.689°	102.21°	4.63	C: (0.1643, 0.5000, 0.2535)	C: (0.163355, 0.500000, 0.248804)
				O: (0.1017, 0.3003, 0.2798)	O: (0.100637, 0.289239, 0.287696)
				(0.2891, 0.5000, 0.1899)	(0.288175, 0.500000, 0.172350)
K_2CO_3 $P12_1/c1$(No.14)[d] f.u. = 4	a = 5.63961	5.76055	2.14	K: (0.2418, 0.0831, 0.2148)	K: (0.241092, 0.081862, 0.195855)
	b = 9.8312	9.90478	0.75	(0.7391, 0.2602, 0.9720)	(0.740909, 0.267167, 0.974545)
	c = 6.83407	7.18110	5.08	C: (0.2455, 0.4174, 0.2489)	C: (0.250376, 0.416094, 0.255014)
	β = 98.703°	97.30°	−1.42	O: (0.7368, 0.0430, 0.2014)	O: (0.737693, 0.042671, 0.194517)
				(0.0631, 0.3488, 0.2770)	(0.063280, 0.346453, 0.276849)
				(0.4147, 0.3609, 0.1718)	(0.424794, 0.359532, 0.186594)

[a]From Ref. 40.
[b]From Ref. 42.
[c]From Ref. 47.
[d]From Ref. 46.

several phases at different temperature ranges,[45–47] here in this study, we only deal with their most stable phases:[29] β-Na_2CO_3 in monoclinic with space group C2/m (#12)[47] (Fig. 1(c)) and monoclinic phase of K_2CO_3 with space group $P2_1/c$ (#14) (Fig. 1(d)).[46] In Table I, we also listed their experimental crystal structural constants as well as our optimized results.

From Fig. 1 and Table I, it can be seen that there are eight f.u. in Na_2ZrO_3 unit cell and four f.u. in other three unit cells. In Na_2ZrO_3, each Zr atom coordinated with six O and each O coordinated with two Zr. Along *c* axis, the connected [ZrO_3] groups form planar layers and separated by Li layers. In [ZrO_3] layer, Zr is in the middle, the bonded O located both sides of Zr, and the Li atoms locate between two Zr, as shown in Fig. 1(a). Similar to Na_2ZrO_3, in K_2ZrO_3 as shown in Fig. 1(b), the [ZrO_3] group also connects to each other. Instead of forming planar layer, they form into $[ZrO_3]_n$ chains. Each chain is surrounded by K atoms. In the case of Na_2CO_3 and K_2CO_3 as shown in Figs. 1(c) and 1(d), the $[CO_3]^-$ groups do not connect to each other and are separated by Na^+ or K^+ ion. From Table I, one can see that the deviations of our optimized structures of Na_2ZrO_3 and K_2ZrO_3 from the corresponding experimental measurements are less than 1.5%. However, large deviations on the angle of Na_2CO_3 and on constant *c* of K_2CO_3 were obtained.

The calculated band structures of M_2ZrO_3 and MCO_3 (M = Na, K) are shown in Fig. 2. It can be seen from Figs. 2(a) and 2(b) that the band structures of Na_2ZrO_3 and K_2ZrO_3 are quite different. Na_2ZrO_3 has two valence bands (VBs), while K_2ZrO_3 has three VBs. The calculated band gap of Na_2ZrO_3 is an indirect one, located between **Γ** and **Z** high symmetric points with the value of 4.339 eV, while the calculated band gap of K_2ZrO_3 is direct with the values of 3.641 eV. They are both insulator materials with large band gaps. As described in our previous work,[27,35] the DFT calculation underestimated the excited-state energy. The calculated band-gaps are usually smaller than the experimental measurements, although currently there is no experimental value available for comparison. The calculated band-gaps, the widths of VBs and the gaps between the VBs of M_2ZrO_3 are summarized in Table II.

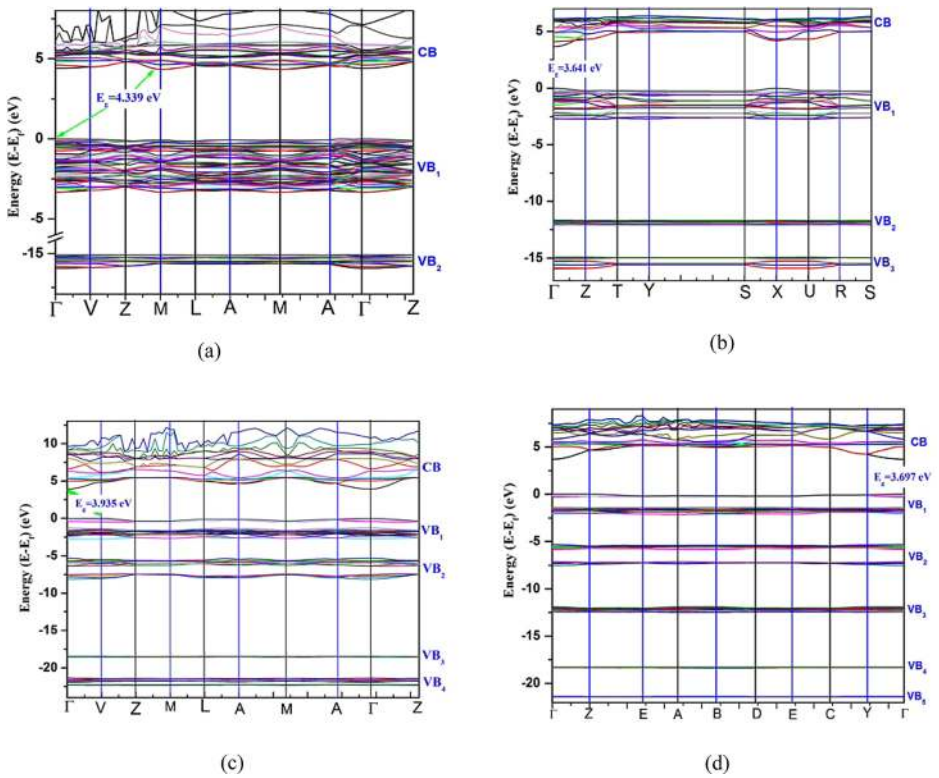

FIG. 2. The calculated electronic band structures: (a) Na_2ZrO_3; (b) K_2ZrO_3; (c) Na_2CO_3; (d) K_2CO_3.

TABLE II. The calculated band gaps and valance band widths of M_2ZrO_3 and M_2CO_3 (M = K, Na, Li) and their corresponding DFT total energies (E^{DFT}), the zero point energies (E_{zp}), and the entropies (S) at T = 298 K from phonon calculations.

Crystal	VB_3 width (eV)	Gap between VB_3 and VB_2 (eV)	VB_2 width (eV)	Gap between VB_2 and VB_1 (eV)	VB_1 width (eV)	Band gap (eV)	E^{DFT} (eV/f.u.)	E_{zp} (kJ/mol)	Entropy (J/mol K)
K_2ZrO_3	0.973	2.839	0.487	8.921	2.757	3.641 (direct)	−40.32835	28.485	168.654
Na_2ZrO_3			0.943	11.837	3.259	4.339 (indirect)	−41.56924	34.497	119.319
Li_2ZrO_3[a]			1.01	11.695	3.73	3.898 (indirect)	−43.76850	36.108	101.88
									91.63[c]
K_2CO_3	0.639	4.370	2.132	5.197	2.158	3.697 (direct)	−36.90480	44.683	160.121
									155.50[c]
Na_2CO_3	0.119	10.466	2.735	2.616	2.736	3.935 (indirect)	−37.29272	47.118	134.685
									138.783[c]
Li_2CO_3[b]	0.117	10.276	3.49	2.102	2.51	5.10 (direct)	−39.55190	57.807	93.615
									90.169[c]
ZrO_2[a]			1.51	10.971	4.94	3.76 (direct)	−28.73057	20.102	51.30
									50.39[c]

[a]Taken from Ref. 14.
[b]α-phase Li_2CO_3 taken from Ref. 27.
[c]Taken from HSC Chemistry package.[48]

As shown in Figs. 2(c) and 2(d), the calculated band structures of Na_2CO_3 and K_2CO_3 have some similarities with several VBs. The calculated band gap of Na_2CO_3 is an indirect one, located between **Γ** and **V** high symmetric points with the value of 3.935 eV, while the calculated band gaps of K_2CO_3 is direct with the values of 3.697 eV. Within their VB_1 and VB_2, there are some small gaps. In Na_2CO_3, the width of VB_1 is 2.736 eV in which a 0.714 eV gap was found and divided the VB_1 into two sub-VBs with widths of 0.595 eV and 1.427 eV, respectively. And its width of VB_2 is 2.725 eV in which a 0.952 eV gap was found and divided the VB_2 into two sub-VBs with widths of 1.070 eV and 0.713 eV, respectively. Similar to Na_2CO_3, in K_2CO_3 the widths of its VB_1 and VB_2 are 2.158 eV and 2.132 eV, respectively. With a gap of 1.172 eV, its VB_1 was separated into two sub-VBs with values of 0.240 eV and 0.853 eV. And by a gap of 1.386 eV its VB_2 was also divided into two sub-VB_2 with the widths of 0.533 eV and 0.426 eV, respectively. As shown in Figs. 2(c) and 2(d), at low energy range (-22 eV ~ -10 eV), Na_2CO_3 has another two bands (VB_3, VB_4) while K_2CO_3 has three

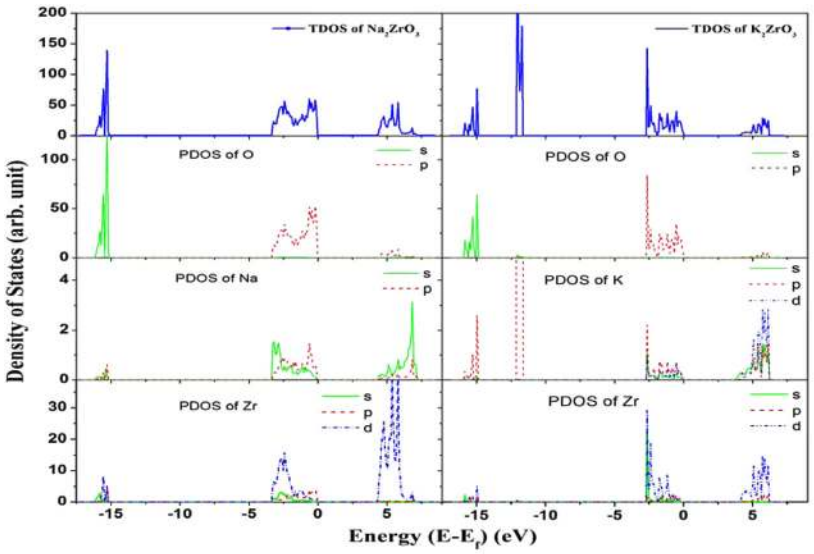

(a)

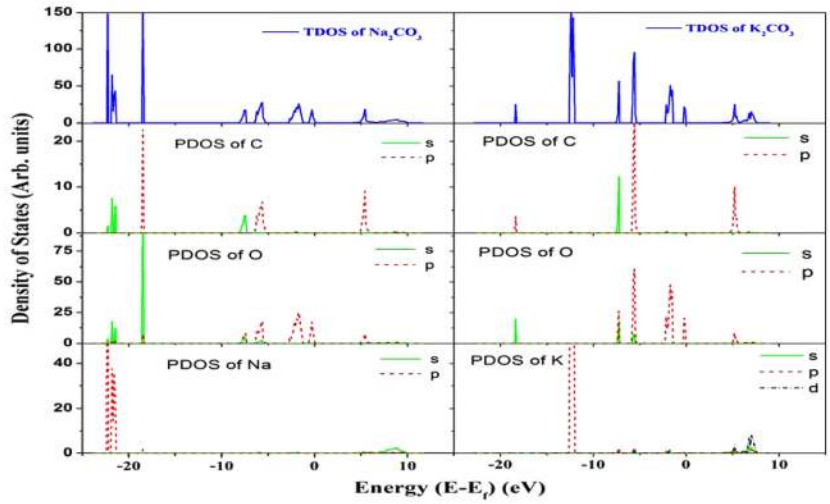

(b)

FIG. 3. The calculated electronic TDOS and projected PDOS: (a) Na_2ZrO_3 and K_2ZrO_3; (b) Na_2CO_3 and K_2CO_3.

bands (VB_3, VB_4, and VB_5) with narrow widths. Their band widths and gaps are also summarized in Table II.

Figure 3(a) shows the calculated total density of states (TDOS) and their corresponding atom partial density of states (PDOS) for Na_2ZrO_3 and K_2ZrO_3. In both cases, the *s* orbital of O contributes to the lowest energy VBs of Na_2ZrO_3 (VB_2) and K_2ZrO_3 (VB_3), while its *p* orbitals are mainly contributed to their VB_1. All the *s*, *p*, and *d* orbitals of Zr contribute to both VBs, but its *d* orbitals have higher contributions than its *s* and *p* orbitals. Compared Na_2ZrO_3 to K_2ZrO_3, one can see that in the case of Na_2ZrO_3, the *s* orbital of Na has more contribution to the lower portion of VB_1 and the conduction band (CB) and its *p* orbitals have more contribution to the upper portion of VB_1, while in the case of K_2ZrO_3, except for having higher contribution over its *s* and *d* orbitals on VB_1, VB_3, and CB, the *p* orbitals of K are mainly contributed to the VB_2. Comparing with Li_2ZrO_3,[14] one can see that the electronic structure of Na_2ZrO_3 is similar to that of Li_2ZrO_3, and both of them are different from that of K_2ZrO_3.

From Fig. 3(b), one can see that in Na_2CO_3 the VB_1 is mainly formed by *p* orbitals of O, VB_2 by interactions of *s* and *p* orbitals of O and C, VB_3 by *s* orbital of O with *p* orbitals of C, and the VB_4 mainly formed by *p* orbitals of Na with *s* orbital of C and O. However, in K_2CO_3, except for VB_1 and VB_2 which are similar to those in Na_2CO_3, the *p* orbital of K forms a single valence band (VB_3), while its *s* and *p* orbitals also involve into other VBs and CB interacting with the *s* and *p* orbitals of C and O.

B. Dynamical phonon properties

As shown in Table I, for Na_2ZrO_3 and Na_2CO_3, there are eight and four f.u. in their unit cells, but their primitive cells have only four f.u. and two f.u., respectively. For both of K_2ZrO_3 and K_2CO_3, since their unit cells are same as their primitive cells, they have four f.u. Therefore, there are 72 phonon modes in Na_2ZrO_3, K_2ZrO_3, and K_2CO_3, while there are only 36 phonon modes in Na_2CO_3. The calculated phonon dispersions of M_2ZrO_3 and M_2CO_3 (M = Na, K) are shown in Figs. 4(a)–4(d), respectively. In Tables III and IV, we summarize our calculated phonon frequencies of these four solids together with the corresponding irreducible representations. It can

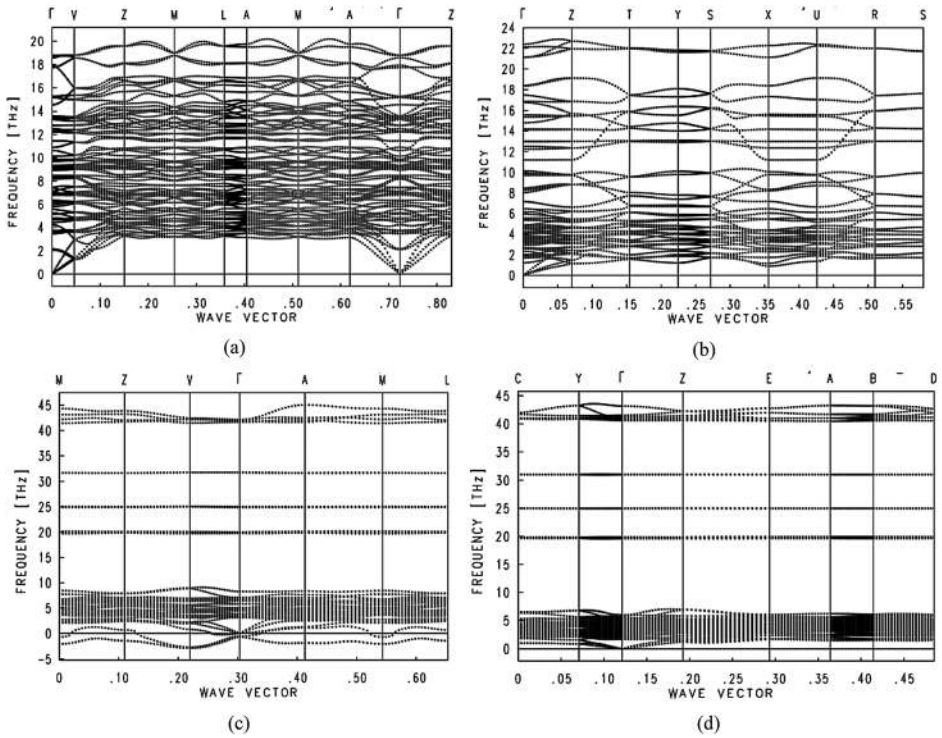

FIG. 4. The calculated phonon dispersions: (a) Na_2ZrO_3; (b) K_2ZrO_3; (c) Na_2CO_3; (d) K_2CO_3.

TABLE III. The calculated frequencies for each irreducible representation vibrational mode of Na_2ZrO_3 and K_2ZrO_3 (unit: cm^{-1}). *R* stands for Raman-active modes and *I* stands for the infrared-active modes.

Na_2ZrO_3 (C12/c1(No.15))				K_2ZrO_3 (Pnma(No.62))			
Modes	Frequencies	Modes	Frequencies	Modes	Frequencies	Modes	Frequencies
A_u(I)	−0.10	B_u(I)	305.34	B_{3u}(I)	0.17	A_u	180.65
B_u(I)	0.10	B_u(I)	309.71	B_{1u}(I)	0.23	B_{3u}(I)	184.59
B_u(I)	0.47	A_u(I)	310.37	B_{2u}(I)	0.43	A_g(R)	198.27
A_g(R)	69.75	A_g(R)	310.71	A_u	40.93	B_{3u}(I)	205.84
B_g(R)	72.08	B_g(R)	323.11	A_g(R)	57.01	B_{1u}(I)	215.34
B_u(I)	116.11	A_g(R)	326.12	B_{2u}(I)	62.61	B_{2g}(R)	215.44
A_u(I)	122.65	B_u(I)	327.62	B_{3g}(R)	66.14	B_{1g}(R)	238.43
B_g(R)	123.98	B_g(R)	329.52	B_{2g}(R)	66.21	B_{2u}(I)	239.79
B_u(I)	125.92	A_u(I)	338.02	B_{1g}(R)	77.12	A_u	267.84
B_g(R)	141.50	B_u(I)	354.74	B_{1g}(R)	85.62	B_{3u}(I)	275.65
A_u(I)	147.60	A_g(R)	363.57	B_{3u}(I)	87.59	A_g(R)	279.15
B_u(I)	155.07	A_u(I)	382.59	A_g(R)	89.19	B_{3g}(R)	282.45
B_u(I)	160.64	B_g(R)	407.10	A_g(R)	97.27	B_{1u}(I)	323.72
A_g(R)	172.21	A_g(R)	409.74	B_{3u}(I)	102.90	B_{2g}(R)	328.85
B_g(R)	175.92	B_u(I)	410.04	A_u	104.64	B_{1u}(I)	331.12
B_g(R)	186.12	A_u(I)	417.21	B_{1g}(R)	107.97	B_{2g}(R)	338.86
A_u(I)	193.33	B_g(R)	425.82	B_{2u}(I)	109.51	B_{3u}(I)	372.92
A_u(I)	200.00	B_u(I)	427.08	B_{1u}(I)	112.44	A_g(R)	373.11
B_u(I)	206.77	A_u(I)	443.79	B_{3g}(R)	115.31	A_u	408.47
B_u(I)	212.17	B_g(R)	444.80	B_{1u}(I)	117.34	B_{3g}(R)	417.58
A_g(R)	226.98	B_u(I)	445.33	A_u	119.38	B_{2u}(I)	433.02
B_g(R)	231.52	A_g(R)	445.33	B_{1g}(R)	122.82	B_{1g}(R)	434.82
B_u(I)	235.23	B_u(I)	447.56	B_{2u}(I)	127.72	B_{3g}(R)	470.85
A_g(R)	237.66	A_u(I)	450.30	B_{2g}(R)	128.15	A_u	473.55
A_u(I)	247.03	A_g(R)	451.30	A_u	132.66	B_{2u}(I)	493.63
B_g(R)	248.60	B_g(R)	453.54	B_{3g}(R)	133.99	B_{1u}(I)	512.67
A_u(I)	272.41	B_u(I)	485.49	A_g(R)	134.76	B_{2g}(R)	519.61
A_g(R)	274.92	B_g(R)	505.37	B_{3u}(I)	139.43	B_{1g}(R)	558.90
B_u(I)	276.65	B_u(I)	506.97	B_{2g}(R)	140.53	A_g(R)	562.64
A_u(I)	278.52	A_u(I)	508.44	B_{1g}(R)	141.89	B_{3u}(I)	582.02
B_g(R)	278.72	A_g(R)	508.44	B_{3g}(R)	149.90	B_{2g}(R)	612.04
B_u(I)	283.09	A_g(R)	591.49	B_{2g}(R)	150.93	B_{1u}(I)	614.14
A_g(R)	298.06	A_u(I)	598.00	B_{1u}(I)	157.00	B_{1u}(I)	704.50
A_u(I)	304.00	B_g(R)	619.74	B_{2u}(I)	162.61	B_{2g}(R)	705.80
B_g(R)	304.37	A_u(I)	626.59	A_g(R)	162.64	A_g(R)	737.99
B_g(R)	305.00	A_g(R)	627.25	B_{3g}(R)	177.55	B_{3u}(I)	746.36

be seen from Fig. 4(c) that only in Na_2CO_3 along the wave-vector there are two soft modes which correspond to the one type of O displacements. In other three solids (Figs. 4(a), 4(b), and 4(d)), no obvious soft mode was found.

The calculated phonon density of states of M_2ZrO_3 and M_2CO_3 (M = K, Na, Li) is shown in Figs. 5(a) and 5(b), respectively. Summarizing with our previous results on Li_2ZrO_3,[14] overall, from K to Na to Li, the frequencies peaks of M_2ZrO_3 and M_2CO_3 are shifted to high frequencies due to the molecular weight decreased from K to Li.

The calculated phonon free energy of each solid versus temperature is shown in Figure 6(a), from which the zero-point energies (E_{zp}) can be obtained and are listed in Table II. In order to compare their properties of capturing CO_2, the thermodynamic properties of Li_2ZrO_3

TABLE IV. The calculated frequencies for each irreducible representation vibrational mode of Na_2CO_3 and K_2CO_3 (unit: cm^{-1}). *R* stands for Raman-active modes and *I* stands for the infrared-active modes.

Na_2CO_3 (C12/m1(No.12))		K_2CO_3 ($P12_1/c1$(No.14))			
Modes	Frequencies	Modes	Frequencies	Modes	Frequencies
B_g(R)	−23.38	B_u(I)	−0.17	A_g(R)	158.37
A_u(I)	−21.05	B_u(I)	0.10	B_u(I)	161.04
B_u(I)	−0.33	A_u(I)	0.13	A_u(I)	161.77
A_u(I)	0.57	A_g(R)	53.87	A_g(R)	168.75
B_u(I)	0.83	A_g(R)	64.08	B_u(I)	172.05
B_g(R)	104.47	A_u(I)	69.51	A_u(I)	176.95
A_u(I)	110.41	B_u(I)	75.12	B_g(R)	178.92
B_u(I)	113.21	B_g(R)	82.65	B_u(I)	181.15
A_g(R)	114.11	A_g(R)	82.89	A_g(R)	181.59
B_g(R)	126.39	B_g(R)	84.59	B_g(R)	184.82
A_u(I)	127.02	A_u(I)	87.92	A_u(I)	188.56
A_g(R)	131.05	B_u(I)	91.33	B_g(R)	200.10
B_u(I)	148.07	A_g(R)	93.80	A_u(I)	653.63
A_g(R)	154.74	A_u(I)	98.70	A_g(R)	654.00
B_u(I)	164.81	B_g(R)	99.00	B_u(I)	656.30
B_g(R)	168.05	B_u(I)	99.50	B_g(R)	656.44
B_u(I)	192.99	B_g(R)	105.90	A_u(I)	659.97
A_g(R)	193.86	A_g(R)	109.04	B_u(I)	660.20
A_u(I)	213.01	A_u(I)	116.31	A_g(R)	660.97
B_u(I)	220.01	A_g(R)	117.14	B_g(R)	662.74
A_g(R)	222.45	B_g(R)	117.88	B_u(I)	831.85
B_u(I)	235.46	A_u(I)	123.08	A_u(I)	832.12
A_u(I)	236.09	A_g(R)	124.32	A_g(R)	833.65
B_u(I)	275.95	B_g(R)	125.88	B_g(R)	834.25
A_u(I)	659.70	B_u(I)	128.18	B_u(I)	1034.09
B_g(R)	661.31	B_u(I)	131.29	B_g(R)	1034.42
B_u(I)	666.94	A_g(R)	133.62	A_u(I)	1034.79
A_g(R)	667.38	A_u(I)	134.39	A_g(R)	1035.59
B_u(I)	829.02	A_g(R)	140.43	A_u(I)	1353.30
A_g(R)	835.45	B_u(I)	140.76	A_g(R)	1358.17
B_u(I)	1060.24	B_g(R)	141.09	B_g(R)	1366.71
A_g(R)	1060.34	B_g(R)	143.90	B_u(I)	1367.91
B_g(R)	1389.75	A_u(I)	147.93	A_u(I)	1371.08
B_u(I)	1396.49	B_u(I)	148.40	A_g(R)	1377.75
A_u(I)	1398.63	B_g(R)	155.44	B_g(R)	1385.52
A_g(R)	1405.90	A_u(I)	156.04	B_u(I)	1440.75

and Li_2CO_3 are also shown in the same figure.[27] As one can see the zero-point energies of these solids are significant and must be included into the predicting their thermodynamic properties (Eq. (3)). Fig. 6(b) shows the calculated entropies of these solids versus the temperatures. Obviously, at 0 K, their entropies are zero and increase with increasing temperature. As shown in Table II, similar to other studied solid sorbents,[29] our calculated entropies of these three solids at room temperature are quite close to the experimental measured values, which indicate that our theoretical approach can achieve reasonable results and, therefore, can be used to evaluate other unknown systems. By including these free energies and entropies at different temperatures into Eqs. (2) and (4), the thermodynamic properties of the reactions of M_2ZrO_3 (M = K, Na, Li) capturing CO_2 can be evaluated as described in Sec. III C.

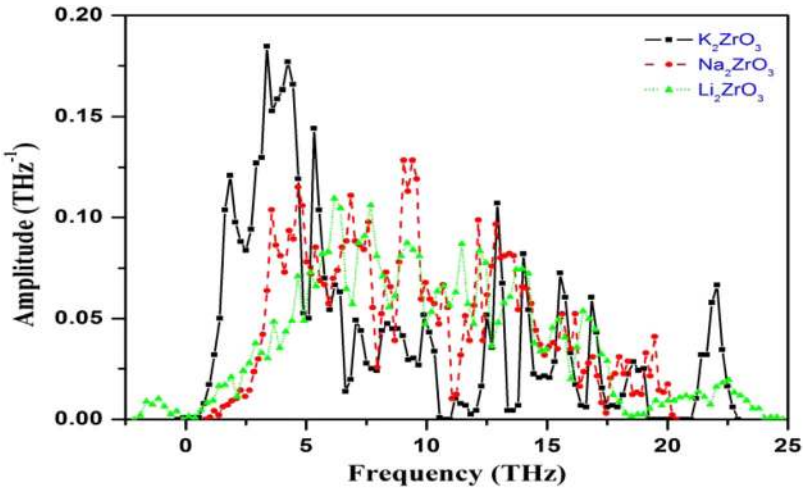

(a)

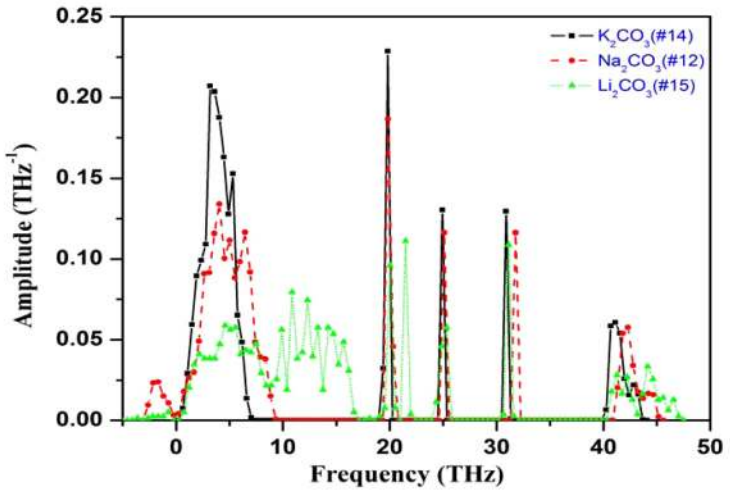

(b)

FIG. 5. The calculated phonon total density of states: (a) M_2ZrO_3; (b) M_2CO_3, M = K, Na, Li.

C. Capabilities of Na_2ZrO_3 and K_2ZrO_3 capture CO_2

Experimental investigations showed that the alkali metal zirconates are good candidates of solid sorbents for CO_2 capture because they have large CO_2 sorption capacity, infinite CO_2/N_2 or CO_2/H_2 selectivity, good reversibility, and high operating temperatures.[8,10–12,16] According to Eq. (4), the calculated heat of reaction (enthalpy change) for reactions of $M_2ZrO_3 + CO_2 = M_2CO_3 + ZrO_2$ (M = K, Na, Li) versus the temperatures is plotted in Fig. 7(a) and also summarized in Table V. The thermodynamic properties of ZrO_2 were taken from our previous work.[14] For comparison, the available experimental data for the reaction of Na_2ZrO_3 capturing CO_2 from HSC Chemistry database[48] are also shown in Fig. 7(a). For the reaction of Na_2ZrO_3 capture CO_2 as shown in Fig. 7(a), the data from HSC Chemistry database have one discontinuity at temperature 725 K, which correspond to the solid-solid phase transition of the product Na_2CO_3 at that temperature.[48] However, in the literature, there is no crystal structure available for those high-temperature solid phases of Na_2CO_3. Therefore, as an approximation, we used the structure of its low-temperature phase (<623 K) to represent its structure in

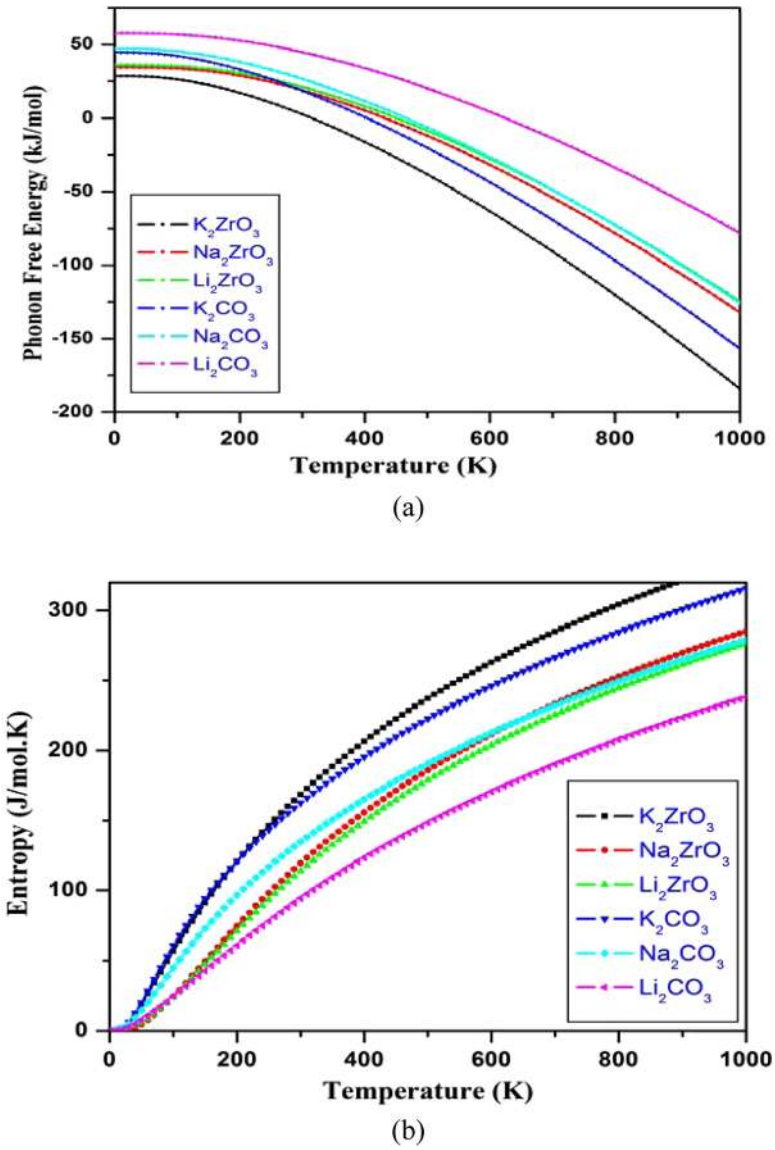

FIG. 6 The calculated thermo-dynamical properties of M_2ZrO_3 and M_2CO_3, where M = K, Na, Li: (a) free energies including zero-point energy versus temperatures; (b) entropies versus temperatures.

high-temperature range, and the temperature effects were partially taken into account by phonon dynamics at different temperatures without specific phase transition. That is why in Fig. 7(a) the simulated enthalpy of the Na_2ZrO_3 capture CO_2 reaction does not have discontinuity compared to the HSC data. As one can see from Fig. 7(a) that overall our calculated heat of reaction for Na_2ZrO_3 is close to the data from HSC Chemistry database within 6 kJ/mol deviation along the temperature range for CO_2 capture. Since there is no experimental data available for K_2ZrO_3, in Fig. 7(a) only our calculated reaction heat of K_2ZrO_3 capturing CO_2 is plotted. For comparison reason, in Fig. 7(a), we also plotted the reaction heat of Li_2ZrO_3 capturing CO_2 from our previous study.[14] From Fig. 7(a), one can see that the reaction of K_2ZrO_3 capturing CO_2 has larger heat of reaction (ΔH), while Na_2ZrO_3 and Li_2ZrO_3 have similar ΔH values with increasing temperatures, which means the reaction of K_2ZrO_3 absorbing CO_2 is stronger than those of Na_2ZrO_3 and Li_2ZrO_3 absorbing CO_2, but the reverse reaction to regenerate K_2ZrO_3 is much harder and needs more energy comparing with the cases of Na_2ZrO_3 and Li_2ZrO_3.

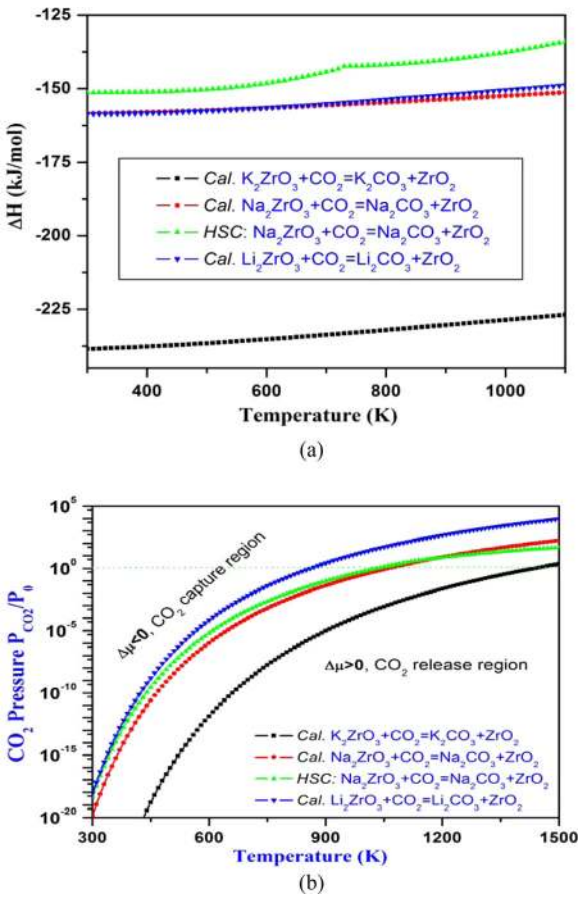

FIG. 7. The calculated thermodynamic properties of the reactions of M_2ZrO_3 (M = K, Na, Li) capturing CO_2: (a) the heat of reaction versus temperature. For the case of Na_2ZrO_3, the data from HSC package are also presented in this figure. The discontinuity of HSC data at 723K indicates solid-solid phase transition of the product Na_2CO_3; (b) the contour plotting of calculated chemical potentials versus CO_2 pressures and temperatures of the reactions. Y-axis plotted in logarithm scale. Only $\Delta\mu = 0$ curve (van't Hoff relation) is shown explicitly. For each reaction, above its $\Delta\mu = 0$ curve, their $\Delta\mu < 0$, which means the alkali metal zirconates absorb CO_2 and the reaction goes forward, whereas below the $\Delta\mu = 0$ curve, their $\Delta\mu > 0$, which means the CO_2 start to release and the reaction goes backward to regenerate the sorbents.

According to Eq. (2), for the reactions of M_2ZrO_3 capturing CO_2, we can explore the relationship among the chemical potential ($\Delta\mu$(T,P)), the temperature, and the COB_2 pressure (P_{CO_2}). This kind of relationship for the reaction (a) is shown in Fig. 7(b) as contour plotting. Only one line for each reaction is plotted explicitly in the Fig. 7(b) on which the $\Delta\mu$(T,P) is zero. Around the line is a good region for the absorption and desorption because of the minimal energy costs at the given temperature and pressure. Above the line, the solid (M_2ZrO_3) is favorable to absorb CO_2 and to form M_2CO_3, while below the line the M_2CO_3 is favorable to release CO_2 and regenerate M_2ZrO_3 solids back.

As described above and shown in Fig. 7, all of these reactions are thermodynamically favorable over a quite wide range of temperatures (<1000 K) and P_{CO_2}, which means that under this temperature range the CO_2 is thermodynamically favored by M_2ZrO_3 (M = Li, Na, K). However, as a CO_2 solid sorbent, it should not only be easy to absorb CO_2 in the first half cycle but also be easy to release the CO_2 from products (M_2CO_3 and ZrO_2, for example) in the second half cycle. The operating conditions for absorption/desorption processes are depending on the pre- and post-combustion technologies. The Department of Energy (DOE) programmatic goal for post-combustion and oxy-combustion CO_2 capture is to capture at least 90% CO_2 with the cost in electricity no more than 35%, whereas the goal in the case of pre-combustion CO_2 capture is to capture at least 90% CO_2 with the cost in electricity no more than 10%.[4,49] Under

TABLE V. The weight percentage of CO_2 capture, the calculated energy change ΔE^{DFT}, the zero-point energy changes ΔE_{ZP}, and the thermodynamic properties (ΔH, ΔG) of the CO_2 capture reactions by alkali metal zirconates. (unit: kJ/mol). The turnover temperatures (T_1 and T_2) of the reactions of CO_2 capture by solids under the conditions of pre-combustion ($P_{CO2} = 20$ bar) and post-combustion ($P_{CO2} = 0.1$ bar) are also listed.

Reaction	Absorbing CO_2 wt. %	ΔE^{DFT}	ΔE_{ZP}	ΔH (T = 300 K)	ΔG (T = 300 K)	Turnover T (K) T_1	Turnover T (K) T_2
$K_2ZrO_3 + CO_2 \leftrightarrow K_2CO_3 + ZrO_2$	20.24	−223.158	5.813	−238.490	−187.884	hT[b]	1285
$Na_2ZrO_3 + CO_2 \leftrightarrow Na_2CO_3 + ZrO_2$	23.76	−140.862	2.236	−158.327	−114.121	1275	925
				−151.403[a]	−105.252[a]		
$Li_2ZrO_3 + CO_2 \leftrightarrow Li_2CO_3 + ZrO_2$[c]	28.75	−146.648	11.311	−158.562	−103.845	1000	780
				−162.69[a]	−113.18[a]		

[a]From HSC-Chemistry database package.[14]
[b]hT means the temperature is higher than our temperature range (1500 K).
[c]Taken from Ref. 48.

pre-combustion conditions, after water-gas shifting, the gas stream mainly contains CO_2, H_2O, and H_2. The partial CO_2 pressure is around 20∼30 bar, and the temperature is around 313∼573 K. To minimize the energy consumption, the ideal sorbents should work at these pressure and temperature ranges to separate CO_2 from H_2. This temperature, denoted T_1, is listed in Table V and is the temperature above which the M_2ZrO_3 cannot absorb CO_2 anymore and will start to release CO_2. This indicates that, during the first half cycle to capture CO_2, the operating temperature should be lower than T_1, whereas the operating temperature may be higher than T_1 (depending on the desired obtained CO_2 pressure) during the second half cycle of sorbents regeneration to release CO_2. For post-combustion conditions, the gas stream mainly contains CO_2 and N_2, the partial pressure of CO_2 is around 0.1∼0.2 bar, and the temperature range is quite different. Currently, in post-combustion CO_2 capture technology, the amine related solvents, carbon, and zeolite (including metal organic framework) based solid sorbents capture CO_2 at low temperature range (<200 °C),[7,50] while oxides (such as CaO and Na_2O) and salts (such as Li_4SiO_4 and Li_2ZrO_3) capture CO_2 usually at high temperature range (>400 °C).[7,14,26,28,29] The turnover temperatures (denoted as T_2) for post-combustion capture by M_2ZrO_3 (M = K, Na, Li) are also listed in Table V.

From Table V and Fig. 7(b), one can see that these three zirconates capture CO_2 up to higher temperatures ($T_1 > 1000$ K) compared with desired pre-combustion condition (313 ∼ 573 K). Therefore, they are not good sorbents for capturing CO_2 in pre-combustion technology. However, they could be used for high-temperature post-combustion CO_2 capture with $T_2 = 1285$ K, 925 K, 780 K for K_2ZrO_3, Na_2ZrO_3, and Li_2ZrO_3, respectively. Obviously, compared to CaO,[7,28] the T_2 of K_2ZrO_3 is still too high to be used for post-combustion technology. This may be part of the reason that there is no experimental work found in the literature for pure K_2ZrO_3 capturing CO_2. Therefore, Na_2ZrO_3 and Li_2ZrO_3 are good candidates for CO_2 sorbents working at high temperature in post-combustion capture technology.

From Table V and Fig. 7(b), one can see that the reverse reaction is not just to dissociate $MB_{2B}CO_3$ but also to regenerate $M_{2B}ZrO_3$ from M_2O by reacting with ZrO_2 which involves net energy gain, and lay down the conditions for $\Delta\mu > 0$ compared with the case of $MB_{2B}O$ (M = K, Na, Li). In other words, the presence of ZrO_2 can destabilize the stable phase of M_2CO_3 and make the reverse reaction to release CO_2 less energy required.[27] Obviously, our results, along with our previous studies,[14,26–29] showed that computational modeling could play an important role and provide guidelines in developing new solid sorbents for CO_2 capture.

IV. CONCLUSIONS

By combining the density functional theory and phonon lattice dynamics, we investigated the electronic structural and phonon properties of M_2ZrO_3 and M_2CO_3 (M = Na, K). The optimized structures of these solids are in a good agreement with experimental measurements.

The calculated band gaps are 4.339 eV (indirect), 3.641 eV (direct), 3.935 eV (indirect), and 3.697 eV (direct) for Na_2ZrO_3, K_2ZrO_3, Na_2CO_3, and K_2CO_3, respectively. In both cases of Na_2ZrO_3 and K_2ZrO_3, the *s* orbital of O contributes to their lowest energy VB_2 in Na_2ZrO_3 and VB_3 in K_2ZrO_3, while its *p* orbitals are mainly contributed to their VB_1. All the *s*, *p*, and *d* orbitals of Zr contribute to both VBs, but its *d* orbitals have higher contributions than its *s* and *p* orbitals. In K_2ZrO_3, the *p* orbitals of K are mainly contributed to the VB_2. The electronic structure of Na_2ZrO_3 is similar to that of Li_2ZrO_3, and both of them are different from that of K_2ZrO_3. The phonon dispersions and phonon density of states for M_2ZrO_3 and M_2CO_3 (M = K, Na) were calculated by the direct method. Overall, from K to Na to Li, the frequency peaks of M_2ZrO_3 and M_2CO_3 are shifted to high frequencies due to the molecular weight decreased from K to Na to Li.

From the calculated thermodynamic properties of M_2ZrO_3 (M = K, Na, Li) reacting with CO_2 through reactions of $M_2ZrO_3 + CO_2 = M_2CO_3 + ZrO_2$, we found that the performance of Na_2ZrO_3 capturing CO_2 is similar to that of Li_2ZrO_3 and is better than that of K_2ZrO_3. Therefore, Na_2ZrO_3 and Li_2ZrO_3 are good candidates of high temperature CO_2 sorbents and could be used for post-combustion capture technology. Pure K_2ZrO_3 is not a good CO_2 sorbent, because it needs much more energy for regenerating at very high temperature.

ACKNOWLEDGMENTS

The author thanks Dr. H. P. Loh for reading the manuscript, Dr. D. C. Sorescu, Dr. D. Luebke, and Dr. H. W. Pennline for their fruitful discussions.

[1]D. Aaron and C. Tsouris, Sep. Sci. Technol. **40**, 321 (2005).
[2]C. M. White, B. R. Strazisar, E. J. Granite, J. S. Hoffman, and H. W. Pennline, J. Air Waste Manage. Assoc. **53**, 645 (2003).
[3]R. S. Haszeldine, Science **325**, 1647 (2009).
[4]J. D. Figueroa, T. Fout, S. Plasynski, H. McIlvried, and R. D. Srivastava, Int. J. Greenhouse Gas Control **2**, 9 (2008).
[5]H. Pfeiffer and P. Bosch, Chem. Mater. **17**, 1704 (2005).
[6]E. Ochoa-Fernandez, H. K. Rusten, H. A. Jakobsen, M. Ronning, A. Holmen, and D. Chen, Catal. Today **106**, 41 (2005).
[7]Q. Wang, J. Luo, Z. Zhong, and A. Borgna, Energy Environ. Sci. **4**, 42 (2011).
[8]G. Pannocchia, M. Puccini, M. Seggiani, and S. Vitolo, Ind. Eng. Chem. Res. **46**, 6696 (2007).
[9]D. J. Fauth, E. A. Frommell, J. S. Hoffman, R. P. Reasbeck, and H. W. Pennline, Fuel Process. Technol. **86**, 1503 (2005).
[10]J. Ida, R. T. Xiong, and Y. S. Lin, Sep. Purif. Technol. **36**, 41 (2004).
[11]K. Essaki, K. Nakagawa, and M. Kato, J. Ceram. Soc. Jpn. **109**, 829 (2001).
[12]K. Nakagawa and T. Ohashi, J. Electrochem. Soc. **145**, 1344 (1998).
[13]B. N. Nair, R. P. Burwood, V. J. Goh, K. Nakagawa, and T. Yamaguchi, Prog. Mater. Sci. **54**, 511 (2009).
[14]Y. Duan, J. Renewable Sustainable Energy **3**, 013102 (2011).
[15]A. Lopez-Ortiz, N. G. P. Rivera, A. R. Rojas, and D. L. Gutierrez, Sep. Sci. Technol. **39**, 3559 (2004).
[16]T. J. Zhao, E. Ochoa-Fernandez, M. Ronning, and D. Chen, Chem. Mater. **19**, 3294 (2007).
[17]L. O. G. Hernandez, D. L. Gutierrez, V. Collins-Martinez, and A. L. Ortiz, J. New Mater. Electrochem. Syst. **11**, 137 (2008).
[18]I. Alcerreca-Corte, E. Fregoso-Israel, and H. Pfeiffer, J. Phys. Chem. C **112**, 6520 (2008).
[19]A. Sandoval-Diaz and H. Pfeiffer, Rev. Mex. Fis. **54**, 65 (2008).
[20]E. Ochoa-Fernandez, T. J. Zhao, M. Ronning, and D. Chen, J. Environ. Eng. Asce **135**, 397 (2009).
[21]V. G. Velderrain, D. B. Jimenez, D. L. Gutierrez, D. D. Vigil, J. S. Gutierrez, A. L. Ortiz, and V. Collins-Martinez, J. New Mater. Electrochem. Syst. **13**, 295 (2010).
[22]M. Olivares-Marin, M. Castro-Diaz, T. C. Drage, and M. M. Maroto-Valer, Sep. Purif. Technol. **73**, 415 (2010).
[23]M. Y. Veliz-Enriquez, G. Gonzalez, and H. Pfeiffer, J. Solid State Chem. **180**, 2485 (2007).
[24]R. Xiong, J. Ida, and Y. S. Lin, Chem. Eng. Sci. **58**, 4377 (2003).
[25]Y. Duan, D. C. Sorescu, and D. Luebke, in *28th Annual International Pittsburgh Coal Conference*, Pittsburgh, 12–15 September 2011.
[26]Y. Duan and K. Parlinski, Phys. Rev. B **84**, 104113 (2011).
[27]Y. Duan and D. C. Sorescu, Phys. Rev. B **79**, 014301 (2009).
[28]Y. Duan and D. C. Sorescu, J. Chem. Phys. **133**, 074508 (2010).
[29]Y. Duan, B. Zhang, D. C. Sorescu, and J. K. Johnson, J. Solid State Chem. **184**, 304 (2011).
[30]S. Cristol, J. F. Paul, E. Payen, D. Bougeard, S. Clemendot, and F. Hutschka, J. Phys. Chem. B **106**, 5659 (2002).
[31]J. H. Wang and M. Liu, J. Power Sources **176**, 23 (2008).
[32]G. Kresse and J. Hafner, Phys. Rev. B **47**, 558 (1993).
[33]G. Kresse and J. Furthmuller, Phys. Rev. B **54**, 11169 (1996).
[34]J. P. Perdew and Y. Wang, Phys. Rev. B **45**, 13244 (1992).
[35]Y. Duan, Phys. Rev. B **77**, 045332 (2008).
[36]H. J. Monkhorst and J. D. Pack, Phys. Rev. B **13**, 5188 (1976).
[37]C. J. Bradley and A. P. Cracknell, *The Mathematical Theory of Symmetry in Solids* (Clarendon, Oxford, 1972).

[38]K. Parlinski, Software PHONON (2006); http://wolf.ifj.edu.pl/phonon/
[39]K. Parlinski, Z. Q. Li, and Y. Kawazoe, Phys. Rev. Lett. **78**, 4063 (1997).
[40]T. J. Bastow, M. E. Hobday, M. E. Smith, and H. J. Whitfield, Solid State Nucl. Magn. Reson. **3**, 49 (1994).
[41]B. M. Gatehouse and D. J. Lloyd, J. Chem. Soc. D: Chem. Commun. **1969**, 727.
[42]B. M. Gatehouse and D. J. Lloyd, J. Solid State Chem. **2**, 410 (1970).
[43]G. Lang, Z. Anorg. Allg. Chem. **276**, 77 (1954).
[44]G. Lang, Z. Anorg. Allg. Chem. **348**, 246 (1966).
[45]M. Dusek, G. Chapuis, M. Meyer, and V. Petricek, Acta Crystallogr., Sec. B: Struct. Sci. **59**, 337 (2003).
[46]Y. Idemoto, J. W. Richardson, N. Koura, S. Kohara, and C. K. Loong, J. Phys. Chem. Solids **59**, 363 (1998).
[47]I. P. Swainson, M. T. Dove, and M. J. Harris, J. Phys.: Condens. Matter **7**, 4395 (1995).
[48]HSC Chemistry software 6.1, Pori: Outotec Research Oy, www.outotec.com/hsc (2006).
[49]DOE-NETL, "Cost and performance baseline for fossil energy plants," Volume 1: Bituminous coal and natural gas to electricty final report, www.netl.doe.gov/energy-analyses/baseline_studies.html (2007).
[50]G. T. Rochelle, Science **325**, 1652 (2009).